

An Evaluation of Cross-Sectional Image Generation Schemes in the Selective Inhibition Sintering (SIS) Process

Matthew Petros*, Payman Torabi*, Behrokh Khoshnevis*

*Daniel J. Epstein Department of Industrial and Systems Engineering, University of Southern California, Los Angeles, CA 90089

Abstract

Selective Inhibition Sintering of metal alloys (SIS-metal) has been proven effective in the additive manufacture (AM) of low resolution bronze parts. The use of high precision inkjet print heads represents a significant advancement in the SIS-metal process. The fabrication of complex three-dimensional metallic parts requires SIS-metal compatible, cross-sectional image processing based on the part boundary profile. Thus, three candidate layer-processing approaches were identified and validated for rudimentary geometries. These approaches were identified from previous research as well as preliminary investigations. The validation criteria is based upon maintaining part integrity, the amount of powder waste produced, processing time, the ability to handle various part geometries, and the ease of access to inhibited regions. Results are discussed for deploying the three candidate layer processing approaches for rudimentary shapes, and a preliminary evaluation is presented for their use on more complex geometries.

Introduction

Additive manufacturing is a term used for the direct manufacture of parts from digital models. AM works by adding material in thin layers from the bottom up, with each layer representing a cross-section of the part [1]. There are various competing technologies in the AM of metal parts such as Direct Metal Laser Sintering (DMLS), Laser Engineered Net Shaping (LENS), Electron Beam Melting (EBM), Selective Laser Melting (SLM) and selective adhesive deposition [2]. There are four common steps to all of these AM technologies:

- 1) A digital model of a part is constructed using one of the various CAD packages (SolidWorks, Alibre, Google SketchUP, and many more).
- 2) The model is imported into a slicing software which generates the profile and/or tool path instructions for each layer of the part.
- 3) A file containing the profile and tool path instructions is transferred to the AM machine, which subsequently builds the part one layer at a time.
- 4) The part is removed and post-processed to achieve desired aesthetic and/or mechanical properties.

Selective Inhibition Sintering

Traditional research in powder sintering has mainly focused on enhancing and speeding the sintering process. Similarly, the metal AM processes mentioned above selectively sinter or fuse particles within each layer's part cross-section. In contrast, the Selective Inhibition Sintering (SIS) process, developed by Dr. Berok Khoshnevis, is based upon the retardation of sintering [2, 3, 4, 5]. The core concept behind the SIS process is the prevention of selected regions of each powder layer from sintering; this is accomplished by treating the regions external to the part in each layer with a sintering inhibitor. In this sense, the SIS process can be considered an inverse to traditional metal AM processes [6].

In the current metal process, a commercial piezoelectric print head is utilized to deposit a liquid chemical solution at the periphery of the part for each layer. Once all of the layers have been completed, the entire part is removed from the machine and bulk sintered in a conventional sintering furnace. The inhibitor deposited at the part's boundary decomposes into hard particles that retard the sintering process. The particles in this region are prevented from fusing, allowing for removal of inhibited boundary sections and revealing of the completed part. Figure 1 is an illustration of the SIS-metal process.

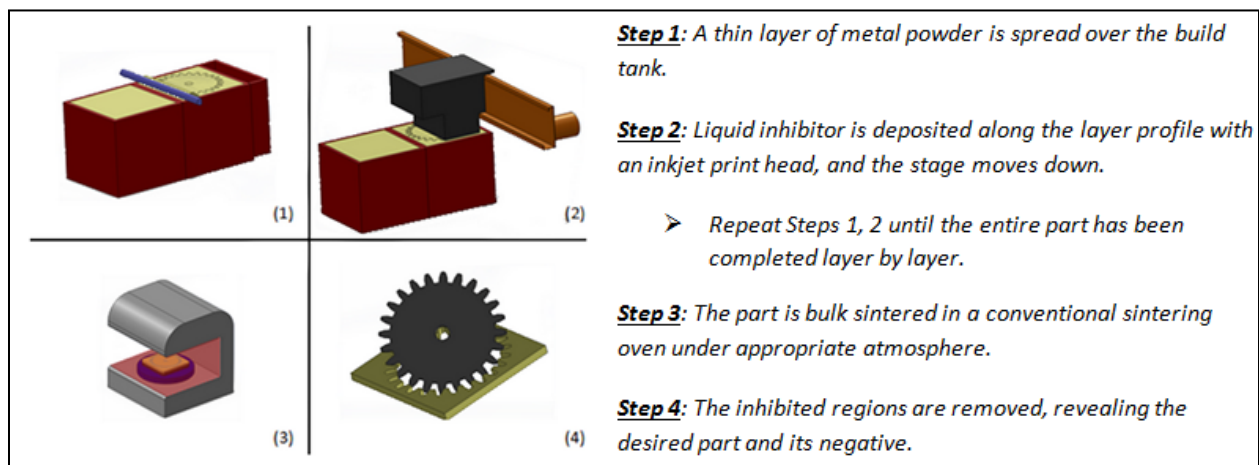


Figure 1: The SIS-metal process

Introduction to Machine Path Planning

Each AM machine needs a machine path generated specifically for that machine's respective process. In all AM processes, with the exception of SIS, the machine path generated traverses the internal cross-section of the part. For example, the standard scanning strategy for the production of parts using SLM first scans the boundary contour and then moves inward to "hatch" the internal cross section for that layer. Various process planning techniques have been developed to accommodate different AM technologies [7]. Factors such as hatch spacing and degree of orientation are important parameters for determining the final mechanical properties of the part [8]. In addition to these parameters, the electron or laser beam speed and layer thickness can have significant effects on part shrinkage and the final size of the part [9].

Previous hatching schemes in SIS, however, had a reverse hatching scheme. Asiabanpour et al. utilized a single nozzle solenoid valve to produce plastic SIS parts by depositing inhibitor solution external to the part periphery [10]. This was done in a raster printing scheme. In 2012, Yoozbashizadeh utilized the same path planning for the successful production of SIS-metal parts [11]. In addition to exploring the use of this hatching scheme, two new hatching schemes are considered for deployment in the high-resolution metal-SIS test bed.

Experimental Setup and Procedures

Hardware

The metal SIS beta prototype machine (Figure 2) was developed at the Center for Rapid Automated Fabrication Technologies (CRAFT) and was utilized for the purposes of this research. The system consists of a three-axis motion system which uses a commercial piezoelectric Epson Workforce 30 print head [12, 13].

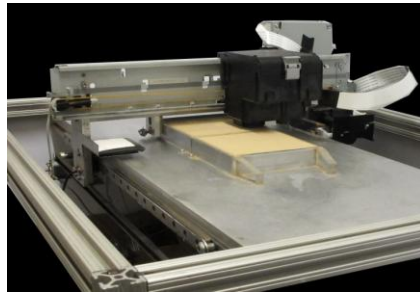


Figure 2: Metal SIS prototype machine.

The inhibitor solution is deposited onto the powder bed by activating two color channels of the printhead simultaneously. These two channels collectively account for one hundred and twenty nozzles. Two colors were used in order to maximize the amount of fluid deposited per pass of the print head. The inhibitor chosen for this research was common table sugar, or sucrose ($C_{12}H_{22}O_{11}$). The inhibitor solution consisted of sucrose dissolved in water and an organic surfactant. Building upon the research of Khoshnevis et al. [6], the metal powder used was a fully alloyed bronze with chemical composition shown in Table 1. The powder particle size has a distribution of 98.7% -325mesh, 1.3% -200/+325mesh as reported by the manufacturer.

Table 1: Chemical composition of bronze as reported by manufacturer

Bronze Chemical Composition	
Copper	90%
Tin	10.00%
Lead	0.025%
Zinc	0.04%
Iron	0.058%
Phosphorous	0.085%

Upon completion of inhibitor deposition, green part was sintered in a programmable, high

temperature Neytech Centurion Qex porcelain furnace. Sintering takes place in a vacuum environment. The sintering profile can be seen in Figure 3.

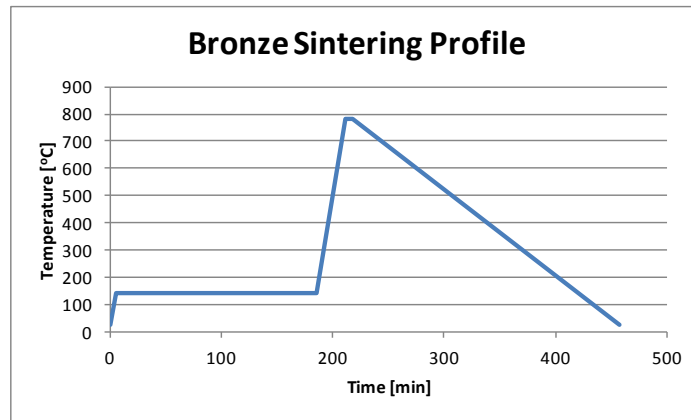


Figure 3: Sintering profile used in experiments

After sintering, the part is ready for post-processing. Separation or removal of inhibited regions was accomplished using a handheld rotary tool with a wire brush attachment typically used for polishing. A Dremel, Model 3000, was used for the purposes of these experiments.

Software

A simple Graphical User Interface (GUI) was developed in Visual C# for ease of implementation of various deposition hatching schemes. Parts were first designed and saved into STL format in SolidWorks CAD software. MeshLab was then used to view and manipulate the STL files when necessary (Figure 4.a&b). Based on the aforementioned research of Asiabanpour et al. and literature review of other AM slicing approaches, the layered images (Figure 4.c) were constructed using a predetermined uniform layer thickness for a given binary STL file format. The layer thickness was determined by the minimum spreadable layer thickness for bronze powder, 120 μm .

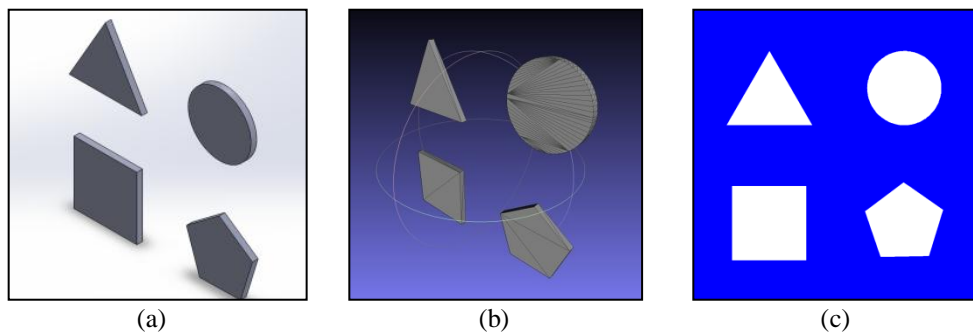


Figure 4: (a) SolidWorks model of simple shapes part file (b) MeshLab view of the associated STL file (c) Sliced image of the STL file

The cross-sectional profiles were obtained from the intersection between the object and regularly spaced planar faces perpendicular to the z direction. The triangles were first sorted by their

respective vertex z values in ascending order. For each layer, two intersections were calculated per triangle to define the cross-sectional profile at a given z height (Figure 5).

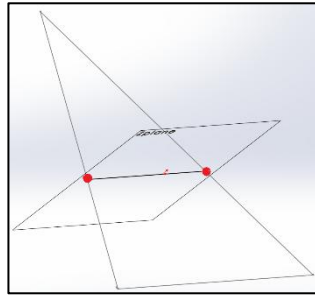


Figure 5: Illustration of two intersection points (red) created by each triangle intersecting a given z plane

Loops in a given cross section were differentiated by a simple algorithm. Each triangle produced a pair of intersections, $[x_1, y_1]$ and $[x_2, y_2]$, which were stored in an irregular sequence. The pairs were first sorted by checking against other pairs in the layer. The sorting process started from the first pair of intersections in the array and searched for an adjacent pair. Once the adjacent pair was found, the next adjacent pair was searched for. This was continued until the loop closed upon itself. If there were points unaccounted for in the same layer, the process would begin again to identify the next loop until all points were accounted for.

Each loop was then ranked using the ray casting method to distinguish between hole and part boundaries; this process determines which side of the boundary will be marked for inhibitor deposition. For example, if the loop represents a part boundary, the area external to the loop will be marked for deposition. If the loop represents the boundary of a hole, the area internal to the loop will be marked for deposition (Figure 6).

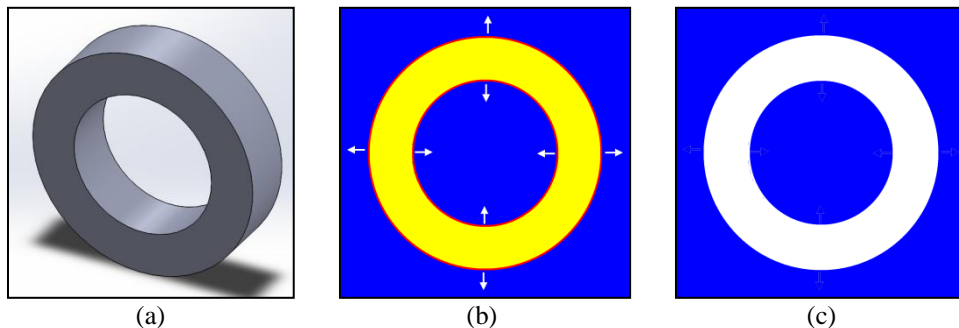


Figure 6: (a) Digital model of a washer (b) Sliced and colored image of a layer cross-section. Yellow represents part, blue represents the filled (printed) region, and red represents the original part boundary location (c) Final sliced image.

An even rank (0, 2, 4...) signifies part boundaries and an odd rank signifies hole boundaries. From these calculations, the images were generated and stored (Figure 6c). For the purposes of this study, images were manually edited depending on the hatching scheme being used. Finally, a print command was sent to the Epson Workforce 30 to begin inhibitor deposition.

Experimental Objectives

Based on the results of preliminary experiments, three hatching schemes were assessed for compatibility with the SIS process. The objectives of these hatching schemes were to:

- A. Minimize powder waste
- B. Maintain part integrity
- C. Minimize process time
- D. Evaluate the ability to handle complex part geometries

Hatching Scheme A (HSA)

Previous research suggested a hatching scheme in which an inhibited base is printed in the first layer. The entire part negative is filled with inhibitor solution for each successive layer afterward (Figure 3c). This hatching scheme is simple to implement and allows for ease of post-processing in that there is direct access to inhibited regions for removal after sintering. However, the large amount of waste is a significant drawback to this hatching scheme. There is currently no cost-effective method for recycling metal powder that has been contaminated by inhibitor solution. In the case of HSA, the entire negative region is contaminated.

The experiment was designed with rudimentary shapes as a proof of concept. The experiment consisted of extruded square, circle, pentagon, and triangle shapes. The same image was repeated over ten layers to create rudimentary shape extrusions. Figure 7a illustrates the results of HSA after sintering.

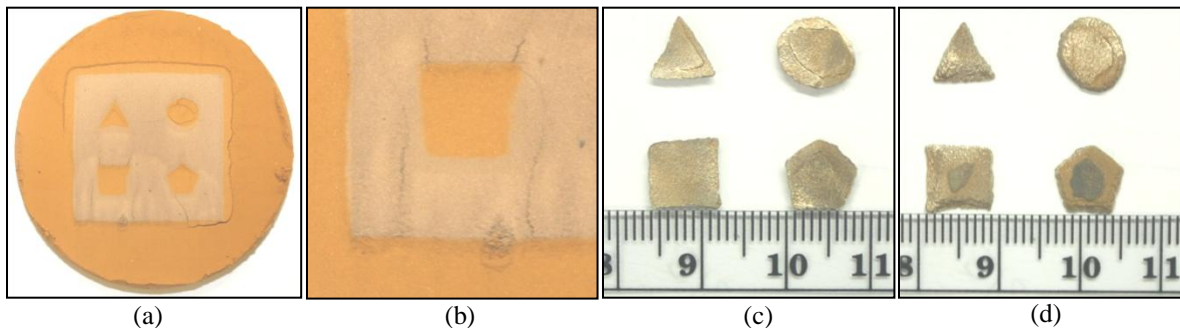


Figure 7: (a) Rudimentary shapes after sintering. The darker colored regions represent the inhibited region (b) Close-up view of flooding in the square shape (c) Front side of final parts after separation from the inhibited region (d) Back side of final parts

Throughout the printing of HSA, it was difficult to control excess fluid deposition. Each layer was visually monitored for signs of flooding. The amount of deposition was adjusted for each layer in an attempt to mitigate part flooding; nonetheless, some layers were flooded in the process. This is evident in Figure 7b, a close-up view of the square shape. Figure 7cd represent the result of the final part after removal of the inhibited regions. The final parts were deformed and exhibited evidence of cracking. This is believed to be a result of excess fluid deposition that penetrated into the part periphery.

As a result of the excess fluid deposited, another drawback was discovered. The excess fluid from layers beneath the surface visibly erupted during the sintering cycle. This is evidenced by the powder ejected in the upper regions of the part. It is believed that the excess water wasn't thoroughly removed during the furnace pre-heat. Consequently, the fluid evaporated rapidly at higher temperatures and was trapped by the liquid and powder above, which eventually led to the eruption.

Hatching Scheme B (HSB)

Based on the results from HSA and differential shrinkage observed by Yoozbashizadeh [11], HSB called for a reduction in the area of inhibited region. This serves two purposes: reducing the powder waste and hampering the potential for cracking. Thus, instead of printing the entire part negative region as in Figure 3c (blue), a thinner boundary profile was designed (Figure 8a). In HSB, an inhibited base was again printed in the first layer. The experiment consisted of an extruded square, circle, pentagon, and triangle with 500 μm boundaries surrounding each shape. A 2 mm thick square perimeter was printed to provide a protective bounding box for ease of transport of the green part. The same image was repeated over ten layers to obtain the desired shape extrusions. Figure 8b illustrates the results immediately after sintering, and Figure 8cd illustrate the results after removal of the inhibited regions.

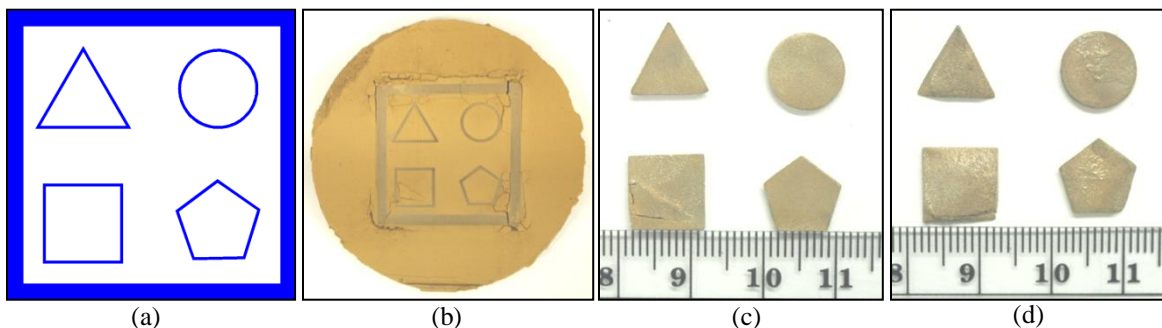


Figure 8: (a) Rudimentary shape design with 480 μm borders and a 2 mm thick printed perimeter (b) Results immediately after sintering (c) Front side of final parts after separation from the inhibited region (d) Back side of final parts

Upon removal from the furnace, the results showed significant visible improvement. The triangle, circle, and pentagon shapes were successfully extracted. However, the square shape exhibited internal cracking. Cracks were observed at the corners of the printed bounding box, as well as within the bounding box (Figure 8b). Slight differential shrinkage was observed at the corners of the bounding box and the triangular part.

Similar to HSA, the extracted rudimentary shapes exhibited signs of excess fluid deposition. This was evidenced during the inhibitor removal. While removing inhibited regions from the back side of the parts, material from within the part itself was easily removed. This signifies that the liquid inhibitor once again penetrated into part.

Hatching Scheme C (HSC)

The results from HSB showed visual improvement for reducing the amount of inhibitor solution deposited. Three of the four original shapes were extracted successfully. However, the integrity of the parts was not maintained. Thus, the HSC design was based on the minimum amount of inhibitor solution allowable for the designed shapes. Torabi, et al. experimentally determined the minimum line thickness for boundary inhibition to be approximately 200 microns. For the SIS process, this is a minimum gap test because the thinnest separable printed line becomes a gap in the finished part after abrasive blasting. Figure 9a represents the sliced image design for the thinnest separable part boundary. The printed perimeter surrounding the shapes in HSB was removed to alleviate excess deformation and stresses induced by water evaporation and shrinkage. In addition, the inhibited base layer was removed in HSC. Instead, the design image (Figure 9a) was printed as the first layer. Figure 9b illustrates the results of the HSC experiment immediately after sintering, and Figure 9cd represent the final part results.

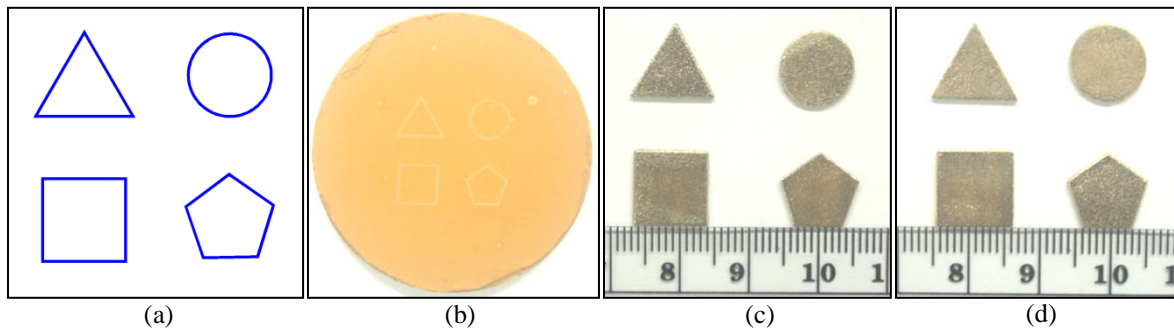


Figure 9: (a) Rudimentary shape design with 200 μm shape borders (b) Results of the HSC experiment immediately after sintering (c) Final part results

The results of HSC again showed significant improvement. There was no visible evidence of cracking within the rudimentary shapes nor external to the parts. Differential shrinkage was not as obvious with the thin border design. In addition, there was no evidence of over penetration of inhibitor within the part periphery. In other words, all deposited inhibitor remained outside of the part as intended.

Discussion

The parameters introduced as experimental objectives were evaluated in Table 2. The ability of a printing scheme to address complex geometries is dependent upon physical access to the inhibited regions after sintering. In this regard, while HSA can theoretically handle the most complex geometries, the amount of powder waste was high and the integrity of the part was very poor. The size of the shapes as well as the verticality of the walls of shapes was a good indicator of shape integrity. HSB had significantly lower powder waste when compared with HSA, but the part integrity was still poor. The integrity was, however, an improvement over HSA. The size of the shapes was closer to the designed size, but the walls were not vertical. In addition, the square shape was cracked internally. HSC produced the lowest amount of powder waste of all, and the

parts maintained a high integrity. The experiment resulted in shapes that were close to their nominal design size and the walls were vertical.

Table 2: Evaluation Criteria for the three hatching schemes.

	Printed Area [mm ²]	Percent Waste	Geometric Complexity	Printing Time [sec/layer]	Access to Inhibited Regions	Part Integrity
HSA	1467	80%	HIGH	19.7	HIGH	LOW
HSB	459	25%	LOW	19.6	LOW	LOW
HSC	63	3%	LOW	16.3	LOW	HIGH

Conclusion and Future Work

Hatching Scheme C presented the most promise for the fabrication of high-quality metallic parts using the new Selective Inhibition Sintering metal prototype machine. However, using HSC only allows for the fabrication of limited part geometries. Complex three-dimensional shapes could not be physically extracted after sintering due to inaccessible inhibited regions. Thus, a new hatching scheme with promising results is under experimentation to address this issue.

References

- [1] Gibson, I., Rosen, D. W., & Stucker, B. (2010). *Additive manufacturing technologies* (pp. 1-8). New York: Springer.
- [2] Kaufui V. Wong and Aldo Hernandez, "A Review of Additive Manufacturing," ISRN Mechanical Engineering, vol. 2012, Article ID 208760, 10 pages, 2012. doi:10.5402/2012/208760
- [3] Khoshnevis, B., Asiabanpour, B., Mojdeh, M., & Palmer, K. (2003). SIS—a new SFF method based on powder sintering. *Rapid Prototyping Journal*, 9(1), 30-36.
- [4] Asiabanpour, Bahram, Kurt Palmer, and Behrokh Khoshnevis. "An experimental study of surface quality and dimensional accuracy for selective inhibition of sintering." *Rapid Prototyping Journal* 10.3 (2004): 181-192.
- [5] Asiabanpour, B. (2003). *An experimental study of factors affecting the selective inhibition of sintering process*. (Order No. 3116659, University of Southern California). *ProQuest Dissertations and Theses*, 168-168 p. Retrieved from <http://search.proquest.com/docview/305297674?accountid=14749>. (305297674).
- [6] Behrokh Khoshnevis, Mahdi Yoozbashizadeh, Yong Chen, (2012) "Metallic part fabrication using selective inhibition sintering (SIS)", *Rapid Prototyping Journal*, Vol. 18 Iss: 2, pp.144 - 153
- [7] Kulkarni P, Marsan A, Dutta D. A review of process planning techniques in layered manufacturing. *Rapid Prototyping J* 2000; 6(1):18–35.
- [8] Stamp, R., Fox, P., O’neill, W., Jones, E., & Sutcliffe, C. (2009). The development of a scanning strategy for the manufacture of porous biomaterials by selective laser melting. *Journal of Materials Science: Materials in Medicine*, 20(9), 1839-1848.

- [9] Senthilkumaran, K., Pandey, P. M., & Rao, P. V. M. (2009). Influence of building strategies on the accuracy of parts in selective laser sintering. *Materials & Design*, 30(8), 2946-2954.
- [10] Asiabanpour, B., & Khoshnevis, B. (2004). Machine path generation for the SIS process. *Robotics and Computer-Integrated Manufacturing*, 20(3), 167-175.
- [11] Yoozbashizadeh, M. (2012). *Metallic part fabrication with selective inhibition sintering (SIS) based on microscopic mechanical inhibition*. (Order No. 3551823, University of Southern California). *ProQuest Dissertations and Theses*, , 187. Retrieved from <http://search.proquest.com/docview/1289076858?accountid=14749>. (1289076858).
- [12] Ink Jet Printers Technical Brief. (2007, May 1). *Epson*
- [13] Epson Micro Piezo Print Head Technology. (2010, January 1). *Epson Exceed Your Vision*.